RSC Advances

ROYAL SOCIETY OF CHEMISTRY

www.rsc.org/advances

Cite this: DOI: 10.1039/c0xx00000x

www.rsc.org/xxxxxx

ARTICLE TYPE

Preparation of a novel PSf membrane containing rGO/PTh and its physical properties and membrane performances

Ahmet Ozgur Saf*[a], Ilker Akin[b], Erhan Zor[c,d] and Haluk Bingol[a]

Received (in XXX, XXX) XthXXXXXXXXX 20XX, Accepted Xth XXXXXXXXX 20XX

DOI: 10.1039/b000000x

Recent advances in the fabrication of nanostructures such as graphene-related materials have received much attention in the membrane technology for the future of water supply. Here we report on the synthesis of reduced graphene oxide/Polythiophene (rGO/PTh) composite material by enzymatic in situ polymerization reaction, which is eco-friendly, and simple way to construct a nanocomposite material. Polysulfone (PSf) mixed matrix composite membranes containing rGO and rGO/PTh were prepared via the phase inversion method. The morphology of membranes was evaluated by various characterization methods, such as SEM, AFM, contact angle and porosity measurements. The performance and antifouling property of membranes were examined in detail. PSf-rGO/PTh membrane showed a significant improvement in the water flux permeability due to the enhancement of the hydrophilicity and porosity. Also, PSf-rGO/PTh membrane exhibited approximately 10 times higher improved water flux than that of the rGO membrane as the pressure was increased. Fouling resistance ratio (FRR) and antifouling property of the membranes were tested by two different protein solutions such as bovine serum albumin (BSA) and Cytochrome c (Ctc). Antifouling and FRR properties of the PSf-rGO/PTh membrane decreased due to not only the interactions between functional groups on membrane surface and fouling materials, but also the morphological properties of membrane.

1. Introduction

The development of ultrathin and nanoporous membranes with high mechanical strength has recently attracted significant interest for broad applications in water purification.[1,2]To date, produced membranes using conventional polymeric materials (polyvinyl chloride,[3] polyaniline[4]) or nanomaterial (ZrO_2,[5], TiO_2,[6]ZnO,[7]AgNP,[8] carbon nanotube[9] and fullerene[10]) enhanced composite membranes have been prepared and they have exhibited good separation performance. In recent years, great effort has been focused on incorporation of carbon-based nanomaterials due to their advantages such as easy to access, high mechanical properties and environmental friendliness.[11]As a rising star of carbon-based nanomaterials, graphene has been a novel and promising material for various applications such as not only in electronics,[12]sensors,[13] solar cells,[14] super capacitors,[15]but also in membrane research.[16,17] Usually, working with modified forms of graphene begins with chemically oxidized graphene (GO) which has recently arisen in membrane research as a fascinating material.[18] However, Ying et al. have stated that due to the low permeability, GO incorporated membrane exhibits relatively low separation efficiency which limits its applications.[19] For this reason, various graphene oxide-polymer hybrid materials have been recently used to arrange nano porosity of the membrane.[20] GO can form a stable aqueous suspension because of the presence of tunable oxygenated functional groups such as carboxyl groups and hydroxyl groups on the surface, side and edge of GO sheets.[21] Hence, when used as the nanofiller, GO possesses strong interactions with the polymer chain and ease to be well-dispersed into the polymer matrix which is intimately related to the antifouling performance.[22] In this regard, graphene-based polymer composites (G-PCs), which can be fabricated using a variety of simple chemical routes such as non-covalent dispersion and in situ polymerization methods, have attracted considerable interest in modern membrane science and technology.[23] Despite the attention graphene has caused, G-PCs have been barely used membrane nanofillers in order to enhance flux and antifouling behavior which are inversely proportional to the thickness and pore size of the membrane.[16] Recently, Akin et al. have proposed a reduced graphene oxide/polyaniline composite material incorporated polysulfone-based composite membrane. They have studied the produced membrane's salt rejection and pure water flux performance and reported that the membrane exhibits high salt rejection value and water flux.[20] Moreover, He et al. have produced a composite membrane using polydopamine-modified graphene oxide sheets incorporated into sulfonated polymer matrix.[24] They investigated its transfer properties and proton-conducting membrane fuel cell performance and stated that the results guarantee the nanocomposite membrane's promising prospects in high-

performance fuel cell. Therefore, it is believed that G-PCs might improve the practical performance of the membrane such as the effects on the surface charge, antifouling and mechanical properties.

For in situ polymerization processes to produce G-PCs, the enzyme-catalyzed reactions have received much attention because the process is simple, one-step, eco-friendly process and does not require strong acidic media[25,26] (i.e. glucose oxidase, which is an oxido reductase enzyme, has been employed for the production G-PCs such as polypyrrole[27] and polyaniline[20]).

The motivation of this study is to report on the synthesis of a novel G-PC and fabrication of polysulfone membrane using it. In this context, rGO/PTh was synthesized via in situ polymerization process, and incorporated in PSf matrix by the phase inversion technique. The performance of the obtained membranes was tested by pure water flux and protein rejection experiments. Also, fouling resistance of the membranes was studied using different protein solutions such as BSA and Ctc.

2. Experimental

2.1. Materials and reagents

All chemicals used in the experiments were purchased from global suppliers and used without further purification. Graphite powder (99.99%), concentrated H_2SO_4 (98%), H_3PO_4, $KMnO_4$ (99%), H_2O_2 (30%), glucose oxidase (GOx), Aspergillusniger (E.C.1.1.3.4.) 295 Umg−1, D-(+)-glucose, thiophene, PSf with Mw-35000, DMF, bovine serum albumin (molecular weight: 66 kD) and Cytochrome c (molecular weight: 12kD) were purchased from Sigma-Aldrich Co., Germany. All aqueous solutions were freshly prepared using Milli-Q ultrapure water.

2.2. Synthesis of rGO/PTh Composite

Graphene oxide (GO) and rGO/PTh composite were synthesized according to literature.[20,27] Briefly, the reduction of GO and occurring polymerization of thiophene to form PTh on the reduced graphene sheets can be explained with a total reaction given in Eq. 1.

$$\mathrm{GO} + \mathrm{Glucose} + \mathrm{Th} \xrightarrow{\mathrm{GOx}} \mathrm{rGO/PTh\ composite} \qquad (1)$$

where, thiophene (Th) is a monomer for polymerization, GOx is the enzyme generating hydrogen peroxide, glucose is a reducing agent of GO.

2.3. Preparation of PSf Membranes

The composite membranes were prepared by the phase inversion technique using PSf as bulk material, DMF as solvent, rGO/PTh composite as additive, and distilled water as non-solvent coagulation bath. The polymer casting solution was prepared by dissolving the polysulfone (15%, w/w) in DMF by vigorous stirring for 12 h to get a homogeneous polymer solution. The desired amount (0.1%, w/w) of rGO or rGO/PTh disbanded in DMF was added. After that, the solution was stirred at 60 ^{0}C for 24 h to obtain a uniform dispersion of rGO or rGO/PTh in polymer casting solution. The casting polymer solutions were sonicated for 10 min to remove air bubbles. Spin coater (Laurell WS-400A-6NPP/LITE) was used for covering a polysulfone layer onto the nonwoven fabric support (Hollytex 3329), being pre-wetted using DMF.[28,29] Subsequently, the covered support was immersed into DI water bath for 10 min at room temperature to induce phase inversion polymerization. The schematic representation of this total procedure is given in Scheme 1.

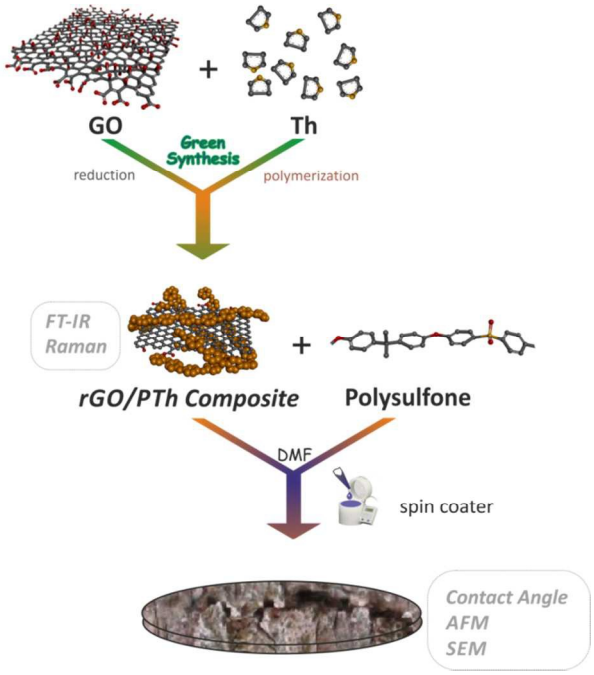

Scheme 1. Schematic diagram for the preparation of the PSf-rGO/PTh composite membrane

2.4. Characterization

Fourier Transform Infrared and Raman Spectroscopy were used to characterize the GO, rGO and rGO/PTh composite. Fourier transformed infrared spectra of the samples were recorded between 550 and 4000 cm^{-1} wave number range using ATR FT-IR spectrometer (PerkinElmer 100 FT-IR). The Raman spectroscopy measurements were performed at room temperature with a Renishaw-inVia spectrometer combined with 514 nm laser. In order to characterize the composite membranes AFM, SEM and CA measurements were used. AFM micrographs were taken using a Park XE7 instrument (scanning speed 1 Hz), and the mean roughness parameter (Ra) was analyzed from three different parts of each composite materials. The structures of composite were examined using a Zeiss EVO-LS10 scanning electron microscope. The membrane samples were cut into 0.5 cm^2, attached with conductive double side tape to steel stabs, and scanned with gold prior to SEM measurements. Contact angle measurements were monitored by a horizontal beam comparator (KSV CAM 200) equipped with video capture. The sessile drop method was used to measure the contact angle of the prepared composite materials[30]. A 4 µL droplet of distilled water was placed on the samples surface, and a magnified image of the droplet was recorded by a digital camera.

2.5. Pilot Plant

The schematic diagram of the pilot system (Prozesstechnick GmbH) is depicted in Fig. 1. The system consists of feed tank including heating/cooling jacket, a diaphragm pump controlled with a frequency converter (flow range: 1.8-12 L min^{-1}; pressure range: max 40 bar) and a flat-sheet membrane housing, which is effective filtration area of 44 cm^2.

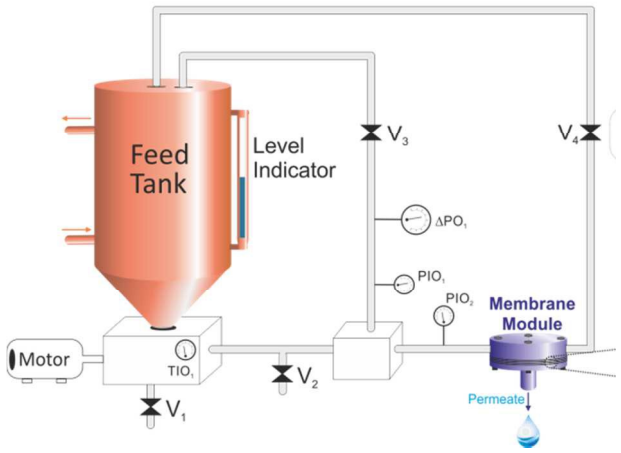

Figure 1. Flow diagram of pilot system;. V_1 and V_2: emptying valve, V_3: pressure regulation valve, V_4: spring loaded valve, PI01 and PI02: pressure gage, DP1: differential pressure indicator, TI01: temperature indicator.

2.6. Permeation and antifouling performance of the membranes

The permeation and antifouling performance of composite membranes were tested by measuring the pure water flux. The experiments were performed at 25°C and 1 MPa. The aqueous solution concentration of BSA and Ctc (0.2 g L^{-1} and 0.05 g L^{-1}, pH=7) was measured by a UV-Vis spectrophotometer (Shimadzu UV-1800). The pure water flux (L $m^{-2}h^{-1}$) was calculated by the following equation:

$$J_{w,1} = \frac{M}{A\Delta t} \quad (2)$$

where M is the volume (L) of the gathered water, A (m^2) and Δt (h) are the membrane area and the permeation time, respectively. The protein rejection R (%) was calculated by equation (3):

$$R(\%) = \left(1 - \frac{C_p}{C_f}\right) x100 \quad (3)$$

where C_p and C_f are the concentrations of the protein in the permeate and feed solutions, respectively.

In order to determine the fouling-resistant behavior of the membrane, the flux recovery ratio (FRR) was evaluated according to the following expression[31]

$$FRR = \left(\frac{J_{w,2}}{J_{w,1}}\right) x100 \quad (4)$$

where $J_{w,1}$ is the initially the pure water flux, using as reference for the membrane permeability and $J_{w,2}$ is the water flux of the cleaned membrane after filtration process. After the pure water flux test, the flux for protein solution J_p (L m^{-2} h^{-1}) was measured at 1 MPa for 6 h. Then, the fouled membranes were washed and immersed in distilled water for 30 minutes. Consequently, $J_{w,2}$ of the cleaned membranes was measured again.

In order to analyze the formation of a cake/gel layer and adsorption onto the membrane surface or within the membrane pores in detail, the fouling mechanism, the total fouling ratio (R_t), reversible fouling ratio (R_r) and irreversible fouling ratio (R_{ir}) were determined using the following equations[32];

$$R_t = \frac{J_{w,1} - J_p}{J_{w,1}} \quad (5)$$

$$R_r = \frac{J_{w,2} - J_p}{J_{w,1}} \quad (6)$$

$$R_{ir} = \frac{J_{w,1} - J_{w,2}}{J_{w,1}} \quad (7)$$

Eventually, R_t is the sum of R_r and R_{ir}.

2.7. Porosity and Pore Size

The overall porosity (ε) of the obtained membranes was measured through the gravimetric method, as defined in the following equation;[31]

$$\varepsilon = \frac{\omega_1 - \omega_2}{Al d_w} \quad (8)$$

where ω_1 and ω_2 are the weight of the wet and dry membrane, A is the membrane effective area (m^2), l is the membrane thickness (m), and d_w is the water density (0.998 g cm^{-3}). The membrane mean pore radius (r_m) was calculated by Guerout−Elford−Ferry [33] equation (Eq. 9) considering the porosity data and the pure water flux.

$$r_m = \sqrt{\frac{(2.9 - 1.75\varepsilon)(8\eta l Q)}{\varepsilon A \Delta P}} \quad (9)$$

where η is the water viscosity (8.9×10^{-4} Pa s), $Q$is the volume of the permeate of pure water per unit time (m^3 s^{-1}), and ΔP is the operational pressure (1 MPa).

3. Results and Discussion

3.1. Characterization of rGO/PTh Composite

FT-IR spectral analysis was performed to characterize the formation of rGO/PTh composite which is the reduction of GO by treating with glucose. Fig. 2a shows the FT-IR spectra of GO and rGO/PTh composite. The spectrum of GO shows the characteristic absorption bands for stretching vibrations of O-H hydroxyl, C=O carbonyl, C−O carboxy, C−O epoxy and C−O alkoxy at around 3211 cm^{-1}, 1719 cm^{-1}, 1401 cm^{-1}, 1221 $cm^{-1}$and 1044 cm^{-1}, respectively[34]. After the reduction process, the other

peaks at oxygen-containing functional groups were significantly weakened whereas the peak at 1719 cm^{-1} belonging to carbonyl groups was nearly disappeared. The results confirm that GO was successfully reduced to rGO moiety.[20] Also, the presence of the peaks at 1526 and 1340 cm^{-1} in the spectrum of rGO/PTh are related to C=C and C–C stretching of thiophene ring, whereas the peaks at 832 and 668 cm^{-1} belong to C–S bond in the thiophene ring.[35,36] The presence of these peaks reveals that PTh obtained by in situ polymerization was successfully settled on the rGO sheets.

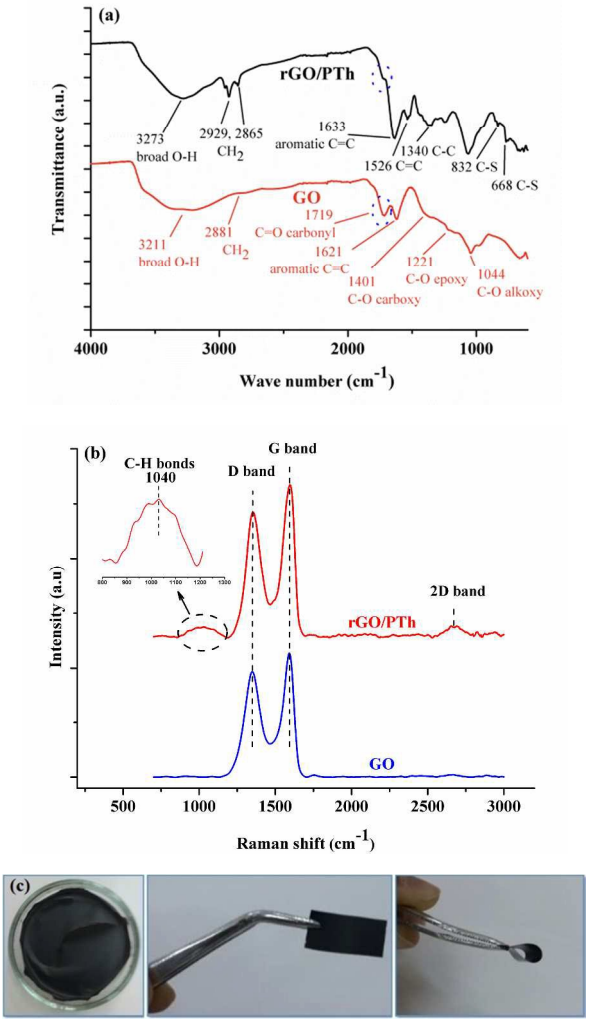

Figure 2. (a) FT-IR spectroscopic analysis of GO and rGO/PTh composite. **(b)** Raman spectra for the GO and rGO/PTh composite. **(c)** Photographes of the rGO/PTh composite.

The successful reduction of oxygen-containing groups in GO and formation of rGO/PTh composite was further confirmed by Raman spectroscopy. Fig. 2b shows the Raman spectra of GO and rGO/PTh. The spectrum of GO indicates two characteristic peaks at 1347 and 1597 cm^{-1} corresponding to D and G bands, which originate from the structural defects and the sp^2 graphitized segment in the structure, respectively.[37]After the reduction with glucose, the D and G bands located at 1353 and 1593 cm^{-1} with a decreased D/G intensity ratio compared to that in GO (I_D/I_G ratio decreased from 0.85 to 0.78). Although the increased I_D/I_G ratio of rGO after reduction has been commonly reported in literature,[38] this decrease indicates that the partial sp^2 domains have been restored[39] and the presence of polyhydrocarbon template on the surface of rGO.[40] Also, the spectrum of rGO/PTh exhibits the characteristic peak, related to the fully in-plane symmetric bending mode of the C–H bonds of the thiophenes, at 1040 cm^{-1} which can be attributed to thiophene structure in the composite.[41,42] In addition to these, Fig. 2c shows photographs of the rGO/PTh composite thin film peeled from the petri dish. The occurring reduction of GO and polymerization of thiophene on rGO sheets gives rise to a color change from brown to black indicating the successfully formation of rGO/PTh composite. The obtained composite shows good flexibility and unbroken properties as can be seen in Fig. 2c.

3.2. Characterization of the Prepared Membranes

The fabricated membranes containing PSf (blank), PSf-rGO and PSf-rGO/PTh were characterized by different methods. To evaluate hydrophilicity and wettability of the membrane surfaces, the contact angle measurements were obtained (Fig. 3). PSf-rGO membrane showed the highest water contact angle of 102.07±0.8°, whereas PSf and PSf-rGO/PTh composite membranes showed water contact angle of 82.8±0.5° and 78.2±1°, respectively [n=3].The increase of the contact angle on the rGO membrane surface can be explained by the hydrophobic character of rGO[43,44], leading to more hydrophobic membrane surface. On the other hand, the resulting PSf-rGO underwent a change from hydrophobic to hydrophilic property due to the PTh molecules, which are coated onto the rGO sheets via π–π interactions.[45] The thiophene groups on the rGO played the key role for increasing hydrophilicity. The improved hydrophilicity can also be explained by the fact that during the phase inversion process, the hydrophilic functional groups migrate spontaneously to the membrane surface, and cause more adsorption of water, which improves membrane water permeability.[46]

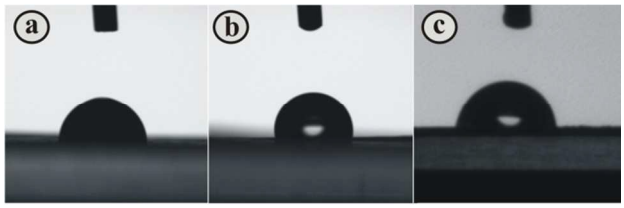

Figure 3. Drop images during contact angle measurements of **(a)**PSf membrane **(b)**PSf-rGO, **(c)**PSf-rGO/PTh composite membrane

The changes of plane surface and cross-section view of the prepared membranes were examined with SEM before and after the modification, which are shown in Fig. 4. It can be seen that the blank PSf membrane surface is relatively smooth (Fig. 4a). The membrane prepared by rGO (Fig. 4b) showed morphological changes compared to blank PSf membrane. The presence of rGO results in porous structure on the membrane surface. The membrane prepared by rGO/PTh (Fig. 4c) exhibited the smaller pore size and higher porosity on the membrane surface. This can be ascribed to the fast exchange of solvent and non-solvent during the phase inversion polymerization.[47]

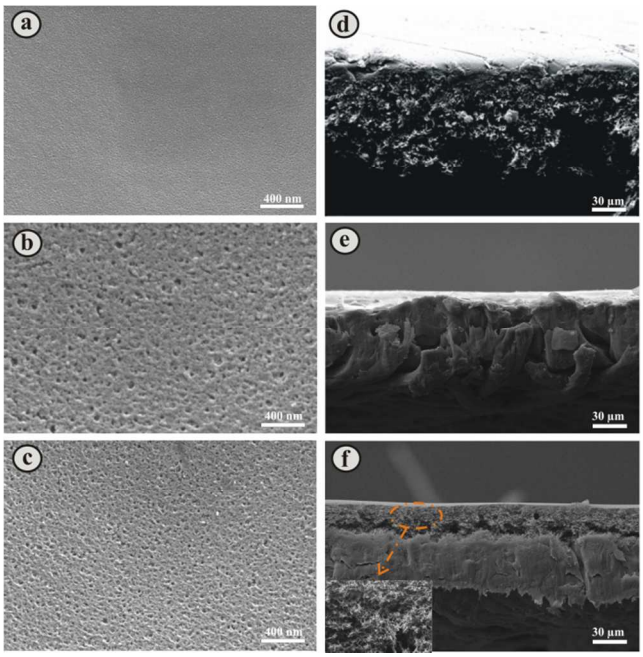

Figure 4.SEM images of surface (a-c) and cross sections (d-f) of PSf (bare), PSf-rGO, and PSf-rGO/PTh membranes

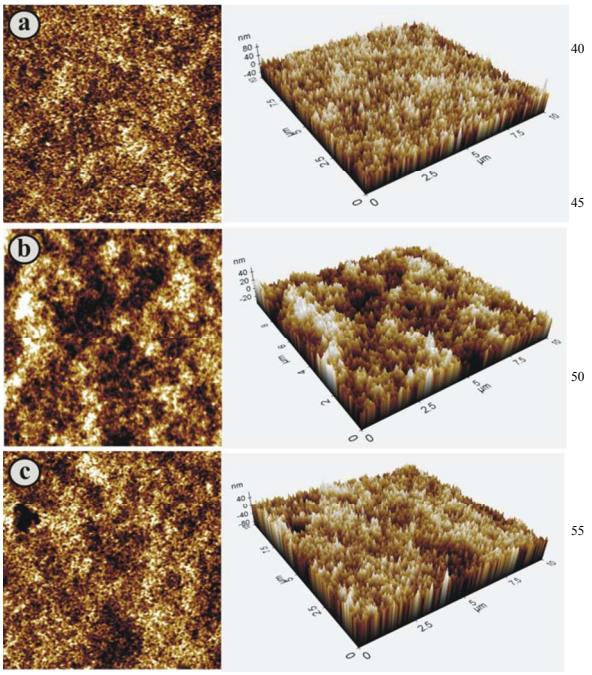

Figure 5.2D and 3D AFM images of the PSf membranes: **(a)**PSf (blank), **(b)**PSf-rGO, **(c)**PSf-rGO/PTh composite membranes

The cross-sectional SEM images of the obtained membranes with different additives such as PSf (blank), PSf-rGO and PSf-rGO/PTh are presented in Figs. 4d, 4e and 4f respectively. The structure of the rGO blended membrane has dense skin layer and slightly irregular microvoids (Fig. 4b), which can be explained by agglomeration behavior of rGO.[48] Yu et al. have reported a similar behavior for hyper branched polyethylenimine graphene blended into PES membranes.[22] The cross-section morphology of the PSf-rGO/PTh membrane is different with sponge-like micro-pores in the top layer of the membrane (Fig. 4f). This can be attributed to processing conditions, which is wetted hollytex fiber using DMF before the casting of the polysulfone layer.[49] When the amount of DMF increases, the non-solvent begins to move into polymer solution film more slowly, while the vitrification front moves more quickly relative to the non-solvent front. As a result of this exchange, the membrane morphology shows formation of sponge-like morphology.[50,51]

Fig. 5 shows two and three dimensional surface AFM images of PSf (blank), PSf-rGO and PSf-rGO/PTh composite membranes, including roughness parameters. In these images, the membrane surfaces are not smooth, and the dark regions indicate valleys or membrane pores. The mean roughness parameter Ra for PSf (blank), PSf-rGO and PSf-rGO/PTh membranes were obtained at 1.22, 3.92 and 1.70 nm respectively. After the addition of rGO, the roughness value of bare PSf membrane increased from 1.22 to 3.92, which is caused by rGO having a hydrophobic character.[20] On the other hand, the addition of rGO-PTh (hydrophilic nature) leads to a reduction in the Ra value of 1.70 nm.

3.3. Porosity and Pore Size

The porosity of the PSf, PSf-rGO and PSf-rGO/PTh membranes was shown in Fig. 6. As can be seen in Fig. 6, the porosity of PSf (blank), PSf-rGO and PSf-rGO/PTh containing membranes was calculated as 45.4, 49.5 and 52.3%, respectively. The increase in porosity arises from the rGO-based material's hydrophilic character that leads to a higher porosity in the membrane surface and thereby improves the water permeability. Besides, the mean pore radius values were found as 11.74, 9.44 and 1.95 nm for the PSf, PSf-rGO and PSf-rGO/PTh membranes, respectively. The results indicate that rGO and rGO/PTh composite membranes have smaller mean pore radius compared to blank PSf membrane because mean pore radius decreases with the addition of rGO and rGO/PTh. This is consistent with the study by Yang et al. who reported that adding appropriate TiO_2 nanoparticles to PSf bulk material can improve its porosity and increase the small pore numbers.[52]

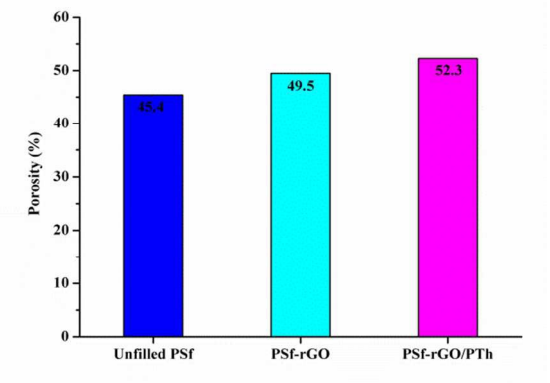

Figure 6. Porosity of the composite membranes

3.4. Membrane Permeation and Antifouling Performance

In order to study the membrane performances in terms of composite membranes containing rGO and rGO/PTh, water flux and protein rejection were examined in detail. The obtained results of pure water flux and protein rejection of the composite membranes were presented in Fig. 7a-c. The composite membrane including rGO/PTh showed higher pure water flux than the PSf-rGO membrane (Fig. 7a). This improvement can be attributed to the increase of hydrophilicity of membrane surface and to the boost of the water permeability by attracting water molecules inside the membrane matrix and facilitate them to move through the membrane.[53] Also, the hydrophilicity effect of rGO/PTh could increase the solvent and non-solvent exchange during the phase inversion technique, therefore leading a membrane with more porous surface and improving the water permeability.[54] Comparing the surface of rGO and rGO/PTh membranes, rGO/PTh membrane has smaller pore size than rGO membrane, whereas it has higher porosity. Although the pore size of rGO/PTh membrane is smaller, its higher porosity gives rise to obtain higher water flux. Eventually, it can be concluded that the porosity of the membrane seems to play a prominent role in good water flux. Also, the water flux permeabilities of PSf-rGO and PSf-rGO/PTh membranes were evaluated under different pressures (Fig. 7b). The increase of pressure led to the increase in water flux permeability for PSf-rGO/PTh membrane, while water flux permeability was slightly increased for PSf-rGO membrane. This is related to the morphological differences including membranes' pore sizes, porosity and structures.[55] In particular, it may have been predicted that higher pressure would lead to deformation of the membrane pores, which could result in the decreasing/unchanging of the water flux. The less change in pore sizes through the increase in pressure can be ascribed to interconnection of the pores with each other inside the sponge-like structure.[56,57]

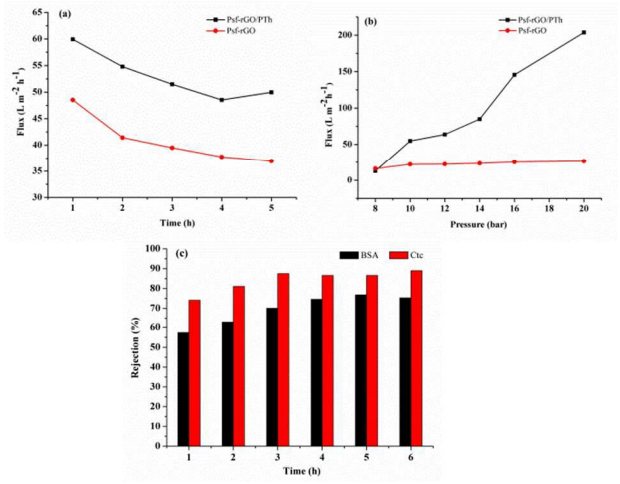

Figure 7. (a) Effect of time on the water flux of PSf-rGO and PSf-rGO/PTh composite membranes at 1MPa operation pressure **(b)** Effect of pressure on the water flux of PSf-rGO and PSf-rGO/PTh composite membranes**(c)** Protein rejection of PSf-rGO/PTh membrane

Protein rejection measurements were carried out with BSA and Ctc protein solutions using a cross flow test system containing rGO/PTh composite membrane. The rejections of the prepared membrane were about 89% for Ctc and about 75% for BSA (Fig. 7c). This can be attributed to the interactions between BSA and Ctc macromolecules and functional groups on the blended membranes surface, as well as the extent of protein retention on membrane surface or pores.[58,59]

The total fouling ratio (R_t), reversible fouling ratio (R_r), and irreversible fouling ratio (R_{ir}) values for the prepared composite membranes were presented in Fig. 8a and 8b. The total fouling resistance of the membranes prepared with the rGO, which is the sum of R_r and R_{ir}, was lower compared to the rGO/PTh membrane. For BSA, R_{ir} value of the PSf-rGO membrane was 7.3% (more than 60% in total fouling) whereas R_{ir} value of the PSf-rGO/PTh membrane was 44.3% (93.1% in total fouling). For Ctc, R_{ir} value of the PSf-rGO membrane was 16.6% (72.6% in total fouling). On the other hand, R_{ir} value of the PSf-rGO/PTh membrane was 67.6% (94.9% in total fouling) (the values are the average of five hours). Contrary to expectations, the rGO composite membrane exhibited higher antifouling properties than that of the rGO/PTh membrane for BSA and Ctc protein solutions. As it is well known, the roughness parameters and hydrophilic properties of the membrane surface are important parameters to describe the fouling ability of membrane.[60] In this point, membrane fouling tendency can be increased with increasing roughness parameter (discussed section 3.2) due to the protein tends to accumulate in the "valleys" of rough membrane surfaces. Safarpour et al.[61] have reported a similar behavior for TiO_2 modified reduced graphene oxide embedding PVDF membrane. On the other hand, we can also speculate that rGO/PTh membrane has further interaction with protein chains by electrostatic attractions and π-π stacking, which can all contribute to the higher R_{ir} values. Due to the less interaction between rGO and protein chains, rGO could reduce the adsorption between membrane and protein. When BSA solution changed with Ctc, having a smaller size and molecular weight, the R_{ir} values of membranes increased. These increases can be related to either the well adsorbed Ctc molecules on the membrane surface or the plugged membrane pores.

Water flux recovery ratio depicted in Fig. 8c can frankly introduce the appropriate recycling properties of the modified membranes. The higher FRR implies the better antifouling property for the membrane. Two different studies were carried out with proteins having different molecular weights. For BSA, the FRR for the rGO blended PSf membrane (91.9%) is higher than the FRR for the membranes prepared with rGO/PTh (62.1%) (the average of 5 h). For Ctc, the FRR for the rGO blended PSf membrane (83.3 %) is higher than the FRR for the membranes prepared with rGO/PTh (45.4%) (the average of 5 h). These results showed the high antifouling property of the PSf-rGO membranes.

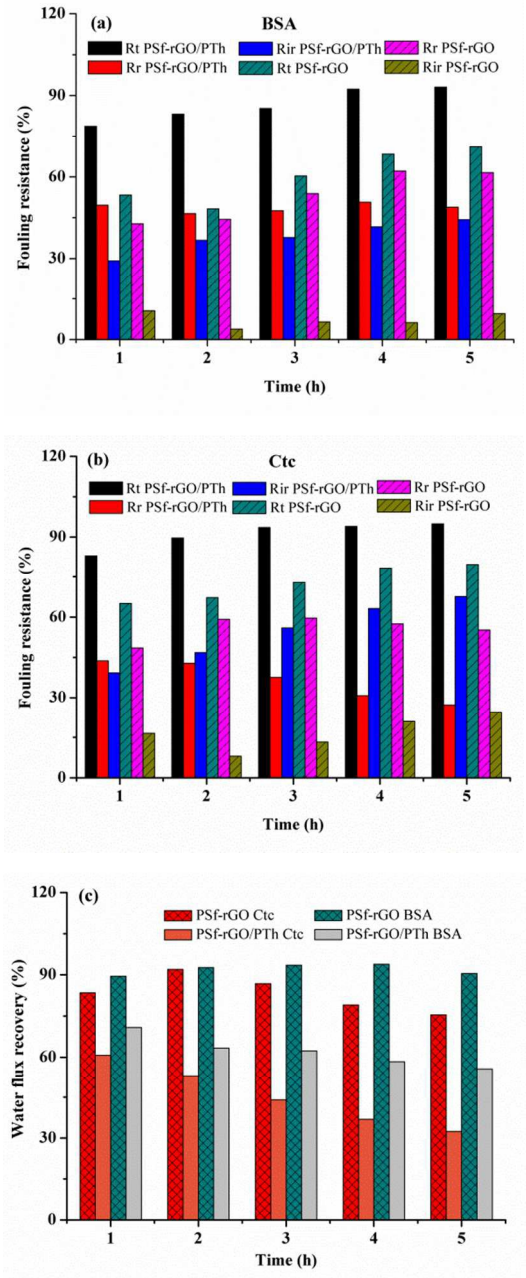

Figure 8. Fouling resistance ratio of composite membranes for **(a)** BSA and **(b)** Ctc; **(c)** water flux recovery of the rGO andrGO/PTh blended PSf membranes after fouling

4. Conclusions

In this study, rGO/PTh composite was synthesized by enzymatic method and characterized using FT-IR and Raman spectral analysis. This composite was used to obtain a novel PSf-based membrane by phase inversion process. The SEM images showed that the prepared composite membrane (PSf-rGO/PTh) possessed sponge-like micro pore structure in top layer of the membrane. The addition of rGO/PTh nanocomposite to the polymer matrix obviously improved the properties and played a favorable role on the characteristics of membrane. The hydrophilicity and porosity of the blended membranes were enhanced by the addition of the rGO/PTh nanocomposite. The rGO/PTh blended PSf membrane also showed significant improvement for promoting water flux permeability with high pressure. PSf-rGO/PTh membranes, which have higher R_{ir} fouling resistance and lower FRR compared to PSf-rGO membrane, can be used for the filtration of water with high pressure in different applications.

Acknowledgements

This work was supported by the Scientific Research Projects of Necmettin Erbakan University (141210001).

Notes and references

[a]*Necmettin Erbakan University, A.K. Education Faculty, Chemistry Department, Konya, Turkey, Fax: +90 332 323 82 25;Tel: +90 332 323 82 20; E-mail:aosaf42@gmail.com; halukbingol@gmail.com*
[b]*Selcuk University, Faculty of Science, Department of Chemistry, Konya, Turkey, E-mail: ilker0997@gmail.com*
[c]*Selcuk University, Institute of Science, Department of Chemistry, Konya, Turkey.*
[d] *Necmettin Erbakan University, A.K. Education Faculty, Science and Technology Department, Konya, Turkey, E-mail: zorerhan@gmail.com*

1 P. Wang, J. Ma, Z. Wang, F. Shi, Q. Liu, *Langmuir*, 2012, **28**, 4776−4786.
2 J.-G. Gai, X.-L. Gong, W.-W. Wang, X. Zhang and W.-L. Kang, *J. Mater. Chem. A*, 2014, **2**, 4023–4028
3 X. Fan, Y. Su, X. Zhao, Y. Li, R. Zhang, J. Zhao, Z. Jiang, J. Zhu, Y. Ma, Y. Liu, *J. Membr. Sci.*, 2014, **464**, 100–109
4 A. A. Qaiser, M. M. Hyland, D. A. Patterson, *J. Membr. Sci.*, 2011, **385–386**, 67–75.
5 R. Pang, X. Li, J. Li, Z. Lu, X. Sun, L. Wang, *Desalination*, 2014, **332**, 60–66.
6 J. H. Pan, X. Zhang, A.J. Du, D. D. Sun, D.D and J. O. Leckie, *J. Am. Chem. Soc.*, 2008, **130**, 11256–11257.
7 L. Shen, X. Bian, X. Lu, L. Shi, Z. Liu, L. Chen, Z. Hou, K. Fan, *Desalination*, 2012, **293**, 21–29.
8 D. Y. Koseoglu-Imer, B. Kose, M. Altinbas, I. Koyuncu, *J. Membr. Sci.*, 2013, **428**, 620–628
9 W. Duan, A. Dudchenko, E. Mende, C. Flyer, X. Zhu and D. Jassby, *Environ. Sci.: Processes Impacts*, 2014, **16**, 1300.
10 K. Tasaki, J. Gasa, H. Wang, R. DeSousa, *Polymer*, 2007, **48**, 4438–4448.
11 H. Huang, Y. Ying and X. Peng, *J. Mater. Chem. A*, 2014, **2**, 13772–13782.
12 B. Standley, W. Bao, H. Zhang, J. Bruck, C. N. Lau and M. Bockrath, *Nano Lett*, 2008, **8 (10)**, 3345-3349.
13 E. Morales-Narvaez, A.-R. Hassan and A. Merkoçi, *Angew. Chem., Int. Ed.*, 2013, **52**, 13779–13783.
14 Z. Liu, J. Li, Z.-H. Sun, G. Tai, S.-P. Lau and F. Yan, *ACS Nano*, 2012, **6 (1)**, 810–818.
15 E. O. Polat and C. Kocabas, *Nano Lett.*, 2013, **13 (12)**, 5851–5857.
16 H. Zhao, L. Wu, Z. Zhou, L. Zhang and H. Chen, *Phys. Chem. Chem. Phys.*, 2013, **15**, 9084– 9092.
17 F. Jin, W. Lv, C. Zhang, Z. Li, R. Su, W. Qi, Q.-H. Yang and Z. He, *RSC Adv.*, 2013, **3**, 21394–21397.
18 P. Sun, M. Zhu, K. Wang, M. Zhong, J. Wei, D. Wu, Z. Xu, H. Zhu, *ACS Nano*, 2013, **7**, 428–437.
19 Y. Ying, L. Sun, Q. Wang, Z. Fan and X. Peng, *RSC Adv.*,2014, **4**,21425–21428.
20 I. Akin, E. Zor, H. Bingol and M. Ersoz, *J. Phys. Chem. B*, 2014, **118**, 5707−5716.

21 J. Lee, H.-R. Chae, Y. J. Won, K. Lee, C.-H. Lee, H. H. Lee, I.-C. Kim, J.-m. Lee, *J. Membr. Sci.*, 2013, **448**, 223–230
22 L. Yu, Y. Zhang, B. Zhang, J. Liu, H. Zhang, C. Song, *J. Membr. Sci.*, 2013, **447**, 452–462.
23 E.-Y. Choi, T. H. Han, J. Hong, J. E. Kim, S. H. Lee, H. W. Kim and S. O. Kim, *J. Mater. Chem.*, 2010, **20**, 1907–1912
24 Y. He, J. Wang, H. Zhang, T. Zhang, B. Zhang, S. Cao and J. Liu, *J. Mater. Chem. A*, 2014, **2**, 9548–9558.
25 A. Ramanavicius, A. Kausaite and A. Ramanaviciene, *Sens. Actuators, B*, 2005, **111–112**, 532–539.
26 A. Kausaite-Minkstimiene, V. Mazeiko, A. Ramanaviciene and A. Ramanavicius, *Biosens. Bioelectron.*, 2010, **26**, 790–797.
27 E. Zor, M. E. Saglam, I. Akin, A. O. Saf, H. Bingol and M. Ersoz, *RSC Adv.*, 2014, **4**, 12457–12466.
28 Z. W. Song, J. M. Zhu, L. Y. Jiang, *J. Membr. Sci.*, 2014, **472**, 77–90.
29 A. Tiraferri, N. Y. Yip, W. A. Phillip, J. D. Schiffman, M.Elimelech, *J. Membr. Sci.*, 2011, **367**, 340–352.
30 Garbassi, F.; Morra, M.; Occhiello, E. Polymer Surfaces From Physics to Technology; Wiley: New York, 1994
31 V. Vatanpour, S. S. Madaeni, R. Moradian, S. Zinadini and B. Astinchap, *Sep. Purif. Technol.*, 2012, **90**, 69–82.
32 D.-G. Kim, H. Kang, S. Han and J.-C. Lee, *J. Mater. Chem.*, 2012, **22**, 8654–8661.
33 N. A. A. Hamid, A. F. Ismail, T. Matsuura, A. W. Zularisam, W. J. Lau, E. Yuliwati, M. S. Abdullah, *Desalination*, 2011, **273**, 85−92.
34 C. Bao, Y. Guo, B. Yuan, Y. Hu, L. Song, *J. Mater. Chem.*, 2012, **22**, 23057−23063.
35 M.G. Han and S.H. Foulger, *Chem. Commun.*, 2005, 3092–3094.
36 X.-G. Li, J.Li, Q.-K. Meng and M.-R. Huang, *J. Phys. Chem. B*, 2009, **113**, 9718–9727.
37 S. Stankovich, D. A. Dikin , R. D. Piner, K. A. Kohlhaas, A. Kleinhammes, Y. Jia, Y. Wu, S. T. Nguyen, R. S. Ruoff, *Carbon*, 2007, **45**, 1558–1565.
38 M. Cheng, R. Yang, L. Zhang, Z.Shi, W. Yang, D. Wang, G. Xie, D. Shi, G. Zhang, *Carbon*, 2012, **50**, 2581 – 2587.
39 S. Some, P. Bhunia, E. Hwang, K. Lee, Y. Yoon, S. Seo, and H.Lee, *Chem. Eur. J.,* 2012, **18**, 7665 – 7670.
40 S.Some, Y. Kim, Y. Yoon, H. J. Yoo, S. Lee, Y. Park & H. Lee, *Scientific Reports, 2013*, 3,1929.
41 J. C. Earles, K. C. Gordon, D. L. Officer and P. Wagner, *J. Phys. Chem. A,* 2007, **111**, 7171- 7180.
42 S. J. Lind, K. C. Gordon, S. Gambhir and D. L. Officer, *Phys. Chem. Chem. Phys.*, 2009, **11**, 5598–5607.
43 E. Singh, Z. Chen, F. Houshmand, W. Ren, Y. Peles, H.M. Cheng and N. Koratkar, *Small*, 2013, **9 (1)**, 75–80.
44 D.-an Zha, S. Mei, Z. Wang, H. Li, Z. Shi, Z. Jin, *Carbon*, 2011, **49**, 5166–5172.
45 J. Zhang and X. S. Zhao, *J. Phys. Chem. C*, 2012, **116**, 5420−5426.
46 V.Vatanpour, M. Esmaeili, M. H.D. A. Farahani, *J. Membr. Sci.*, 2014, **466**, 70–81.
47 V. Vatanpour, S.S. Madaeni, R. Moradian, S. Zinadin, B. Astinchap, *J. Membr. Sci.*, 2011, **375**, 284–294.
48 I. Rosas, S.Collado, A. Gutiérrez, M. Díaz, *J. Membr. Sci.*, 2014,**465**, 27–33.
49 H.-Y. Hwang, D.-J.Kim, Y.-T.Hong, S.-Y. Nam, *Trans. Nonferrous Met. Soc. China,* 2011, **21**, 141-147.
50 P. vandeWitte, P.J. Dijkstra, J.W.A. vandenBerg, J. Feijen, *J. Membr. Sci.*, 1996,**117**, 1–31.
51 R. Baker, Membrane Technology and Applications, 2nd ed.,Wiley, 2004.
52 Y. Yang, H. Zhang, P. Wang, Q. Zheng, J. Li, *J. Membr. Sci.*, 2007, **288**, 231−238.
53 N. Pezeshk, D. Rana, R.M. Narbaitz, T. Matsuur, *J. Membr. Sci.*, 2012, **389**, 280–286
54 S. Zinadini, A. A. Zinatizadeh, M. Rahimi, V. Vatanpour, H. Zangeneh, *J. Membr. Sci.,* 2014, **453**, 292−301.
55 S.H. Yoo, J. H. Kim, J. Y. Jho, J. Won, Y. S. Kang, *J. Membr. Sci.*, 2004, **236**, 203–207.
56 K.M. Persson, V. Gekas, G. Trägårdh, , *J. Membr. Sci.*, 1995, **100**, 155–162.
57 Z. Zhang, Q. An, T. Liu, Y. Zhou, J. Qian, C. Gao, *Desalination*, 2011, **269**, 239–248.
58 M. Hashino, K. Hirami, T. Ishigami, Y. Ohmukai, T. Maruyama, N. Kubota, H. Matsuyama, *J. Membr. Sci.*, 2011, **384**, 157–165.
59 E. Celik, L. Liu, H. Choi, Water Res., 2011, **45**, 5287 -5294
60 D. Rana, T. Matsuura, *Chem. Rev.*, 2010, **110**, 2448−2471.
61 M. Safarpour, A. Khataee and V.Vatanpour, *Ind. Eng. Chem. Res.*, 2014, **53**, 13370−13382.